methane

MDPI

Article

Identifying Monomeric Fe Species for Efficient Direct Methane Oxidation to C_1 Oxygenates with H_2O_2 over Fe/MOR Catalysts

Caiyun Xu *, Qian Song, Nagme Merdanoglu, Hang Liu and Elias Klemm *

Institute of Technical Chemistry, University of Stuttgart, Pfaffenwaldring 55, 70569 Stuttgart, Germany; qian.song@itc.uni-stuttgart.de (Q.S.); nagme.merdanoglu@itc.uni-stuttgart.de (N.M.); hang.liu@itc.uni-stuttgart.de (H.L.)

* Correspondence: caiyun.xu@itc.uni-stuttgart.de (C.X.); elias.klemm@itc.uni-stuttgart.de (E.K.)

Abstract: Exploring advanced catalysts and reaction systems operated at mild reaction conditions is crucial for conducting the direct methane oxidation reaction toward oxygenate products. Many efforts have been put into research on pentasil−type (MFI) zeolites based on mononuclear and/or binuclear iron sites, using H_2O_2 as the oxidant. In this work, we present a modified liquid ion−exchange method to better control Fe loading in a mordenite−type (MOR) zeolite with a Si/Al molar ratio of 9. The optimized Fe/MOR catalyst showed excellent performance in the direct methane oxidation reaction with turnover frequencies (TOFs) of 555 h^{-1} to C_1 oxygenates, significantly better than the reported activity. Multiple comparative experiments were conducted to reveal the mechanism behind the performance. Strikingly, the active sites in the Fe/MOR catalyst were found to be mononuclear iron sites, confirmed by transmission electron microscopy (TEM), ultraviolet−visible diffuse reflectance spectroscopy (UV−vis DRS), and X-ray absorption spectroscopy (XAS). Increasing the iron loading led to the aggregation of the iron sites, which tend to trigger undesirable side reactions (i.e., H_2O_2 decomposition and over−oxidation), resulting in a significant decrease in TOFs to C_1 oxygenates.

Keywords: methane oxidation; monomeric Fe species; mordenite; C_1 oxygenates; hydrogen peroxide

Citation: Xu, C.; Song, Q.; Merdanoglu, N.; Liu, H.; Klemm, E. Identifying Monomeric Fe Species for Efficient Direct Methane Oxidation to C_1 Oxygenates with H_2O_2 over Fe/MOR Catalysts. *Methane* **2022**, *1*, 107–124. https://doi.org/10.3390/methane1020010

Academic Editor: Mateusz Wnukowski

Received: 7 March 2022
Accepted: 20 April 2022
Published: 1 May 2022

1. Introduction

As the primary constituent of natural gas and other fossil reserves, methane is considered essential in the world's energy transition due to its extended availability, affordability, and clean combustion. However, the gaseous nature and uneven regional distribution, often in remote areas, restrict its widespread utilization, especially considering the high cost of traditional pipeline transportation and leakage problems. In addition, methane is an essential greenhouse gas, which is showing rapidly growing environmental hazards in this century. Exploiting an efficient way to convert methane to methanol and other oxygenates, which are transportable, storable, and highly valuable in the chemical market, would be a promising strategy compared to flaring. The main obstacle to achieving applicable transformation lies in the difficulty of activating the robust C−H bond (440 kJ mol^{-1}) [1–3]. The indirect synthesis route adopted in the industry proceeds through syngas generation by methane reforming and requires considerable energy input over multistage processes [4]. The development of direct routes for the conversion of methane into value−added chemicals, especially CH_3OH, is thermodynamically feasible and economically/environmentally favorable. In nature, methane monooxygenase (MMO) enzymes can perform selective direct methane oxidation to methanol (DMTM) under ambient conditions based on Fe−oxo and Cu−oxo clusters as the active sites [5]. Incorporating these metals into zeolitic frameworks with H_2O_2, O_2, and/or H_2O as oxidants can result in biomimetic activity [6,7]. In the past decade, several research groups have made many efforts to elucidate the precise Cu configuration in Cu/zeolites for the stepwise conversion of DMTM using O_2 and/or

H_2O [8]. However, despite the high CH_3OH selectivity, the resulting low yield and repeated heating and cooling steps during one cycle extend the cycle time and limit its applicability.

H_2O_2 has been proved to be a green, environmentally friendly, and highly efficient oxidant for CH_4 oxidation to C_1 oxygenates, including CH_3OH, CH_3OOH, $OHCH_2OOH$, and HCOOH, through a radical reaction pathway under mild conditions (25–100 °C) [9,10]. In 2012, Hammond et al. [10] first reported that the H−ZSM−5 (n−Si/Al = 15) catalyst with 0.014 wt.% Fe impurity exhibited unique activity, with TOFs of up to 2200 h^{-1} toward C_1 oxygenates at 50 °C using H_2O_2 as the oxidant in a batch reactor. Zuo et al. [11] also showed that commercial ZSM−5 (n−Si/Al = 17) with a trace amount (175 ppm) of the Fe impurity showed a considerable methane conversion of 6.5% with a high TOF of 2411 h^{-1} at 100 °C in a fixed−bed reactor. The di−iron complex $[Fe_2(\mu_2-O)_2(OH)_2(H_2O)_2]^{2+}$, analogous to the binuclear Fe found in soluble methane monooxygenase (sMMO), was proposed to be the active site based on a combination of ex situ spectroscopic investigations and density−functional theory (DFT) calculations [10]. Table S1 shows the catalytic performance of the representative catalysts for low−temperature (25–100 °C) methane oxidation with H_2O_2 as the oxidant. Although direct methane oxidation has also been observed on a variety of heterogeneous catalysts, i.e., Fe−NC SACs [9], AuPd/TiO_2 [12], Rh_1/ZrO_2 [13], Rh/CeO_2 [14], CNT@PNC/Ni SAs [15], Cr_1/TiO_2 [16], MIL−53(Fe,Al) [17], and UiO−66(2.5TFA)−Fe [18], no other catalyst has been reported to be as active as the Fe/ZSM−5 catalyst [10]. Therefore, besides MFI, developing other zeolite catalysts as more efficient catalytic systems is necessary.

The zeolite topology is crucial to the activity, which provides the appropriate geometric constraint around Fe or Cu to maintain ultrafine Fe−oxo or Cu−oxo sites that act as active sites. Rationally fabricating active Fe sites in zeolites will significantly promote their activity. It cannot be ruled out that the Fe active sites in H−ZSM−5 are present as monomeric Fe species. In 2021, Luo and coworkers [19] confirmed that mononuclear Fe species were the active sites in 0.1% Fe/ZSM−5 by correlating a wide variety of characterization results with the obtained catalytic performance data. However, compared with a wide array of zeolite frameworks that have been proved to host copper sites, spanning from mononuclear Cu to large clusters ($Cu_4O_4^{2+}$ and $Cu_5O_5^{2+}$) [8], the development of Fe/zeolites and the identification of Fe sites in H_2O_2−mediated DMTM conversion have been limited. Only the Fe/MFI catalyst has received broad interest in the last decade. In 2019, Liu and coworkers [20] reported that an active 0.5 wt.% Fe/MOR−H_2 catalyst synthesized via simple solid−state ion exchange showed around 240 μmol of C_1 oxygenates with 89% selectivity and a TOF of 90 h^{-1}. Although the Fe/MOR catalyst activity with dimeric Fe^{3+} species was certified [20], it still lacks further exploration, which offers a high potential for additional optimizations and an in−depth understanding of the Fe active site.

Herein, a modified liquid ion−exchange method (mIE) adopting $Fe(acac)_3$ (acac = acetylacetonate) as the iron precursor and CH_3CN as the solvent was used to load Fe onto a MOR−type zeolite in a more controlled manner. The advantage of this method is highlighted by comparing it with other traditional loading methods. Catalytic performance was investigated, of which around 0.260 wt.% Fe/MOR exhibited the best yield and TOFs of up to 555 h^{-1} toward C_1 oxygenates. By comparing the catalytic performance with the concentration of Fe sites, as determined from spectroscopic studies, it was proved that mononuclear Fe ions are the active sites for direct methane oxidation, which was further confirmed by XAS. The relative reduction in the performance at higher Fe contents could be ascribed to the aggregation of iron species.

2. Materials and Methods

The source and purity of the chemicals mentioned in the text are listed in Table S2.

2.1. Catalyst Preparation

2.1.1. Different Loading Methods

Fe/MOR(NH_4) catalysts with a nominal 0.5 wt.% Fe loading were obtained by using a commercial NH_4-MOR catalyst with 0.06 wt.% Fe impurity (n−Si/Al = 9, Alfa Aesar) and different Fe precursors: iron (III) nitrate nonahydrate ($Fe(NO_3)_3 \cdot 9H_2O$), iron (III) acetylacetonate ($Fe(acac)_3$), or iron(III) chloride hexahydrate ($FeCl_3 \cdot 6H_2O$). Different methods were employed as follows:

For the modified liquid ion−exchange (mIE) method, 200 mg of NH_4-MOR powder and a certain amount of Fe salts corresponding to a nominal 0.5 wt.% Fe loading (6.3 mg $Fe(acac)_3$; 7.2 mg $Fe(NO_3)_3 \cdot 9H_2O$; 4.8 mg $FeCl_3 \cdot 6H_2O$) were added to 8 mL of CH_3CN in a glass vial. The vials were treated with ultrasound for 2 min and placed in an oven at 85 °C for 24 h. The resulting samples were centrifuged and washed with acetone, deionized water, and acetone sequence and then dried in an oven at 80 °C for 5 h. Finally, they were calcined under an air flow at 500 °C with a heating ramp of 100 °C/h and kept at that temperature for 5 h. The finally obtained catalysts are denoted as $1-0.260Fe/MOR_{mIE}$, $2-0.590Fe/MOR_{mIE}$, and $3-0.150Fe/MOR_{mIE}$ in line with different Fe precursors: $Fe(acac)_3$, $Fe(NO_3)_3 \cdot 9H_2O$, and $FeCl_3 \cdot 6H_2O$, respectively.

For the standard liquid ion−exchange (sIE) method, 200 mg of NH_4-MOR powder and a certain amount of Fe salt (7.2 mg $Fe(NO_3)_3 \cdot 9H_2O$) corresponding to a nominal 0.5 wt.% Fe content were added to 8 mL of deionized water in a glass vial. The following procedure is similar to the above mIE method. The obtained catalyst is denoted as $4-0.510Fe/MOR_{sIE}$.

For the solid−state ion−exchange (SSIE) method, 400 mg of NH_4-MOR powder was mixed and intensively ground with a certain amount of Fe salts corresponding to a nominal 0.5 wt.% Fe (12.6 mg $Fe(acac)_3$; 14.4 mg $Fe(NO_3)_3 \cdot 9H_2O$) in an agate mortar for 1 h under ambient conditions. Then, the obtained homogeneous mixture was calcined under an air flow at 500 °C with a heating ramp of 100 °C/h and kept at that temperature for 5 h. The finally obtained catalysts are denoted as $5-0.524Fe/MOR_{SSIE}$ and $6-0.547Fe/MOR_{SSIE}$ in line with different Fe precursors: $Fe(acac)_3$ and $Fe(NO_3)_3 \cdot 9H_2O$, respectively.

For the incipient wetness impregnation (IWI) method, 200 mg of NH_4-MOR powder was charged into a 25 mL round−bottom flask equipped with a magnetic stirring bar. A certain amount of Fe salt corresponding to a nominal 0.5 wt.% Fe loading (6.3 mg $Fe(acac)_3$; 7.2 mg $Fe(NO_3)_3 \cdot 9H_2O$) was dissolved in a liquid mixture containing 2 mL ethanol/1 mL CH_3CN/0.5 mL H_2O and then added to the flask. The flask was stirred vigorously and then kept at 30 °C for 24 h. The obtained material was then dried at 80 °C for 5 h and calcined under an air flow at 500 °C with a heating ramp of 100 °C/h and kept at that temperature for 5 h. The catalysts are denoted as $7-0.423Fe/MOR_{IWI}$ and $8-0.518Fe/MOR_{IWI}$ in line with different Fe precursors: $Fe(acac)_3$ and $Fe(NO_3)_3 \cdot 9H_2O$, respectively. Alternatively, a certain amount of $Fe(NO_3)_3 \cdot 9H_2O$ corresponding to a nominal 0.5 wt.% Fe loading (7.2 mg) was dissolved in 3.5 mL of deionized water and added to a 10 mL flask containing 200 mg of NH_4-MOR powder. Subsequently, the flask was submerged in a 50 °C water bath under vigorous stirring for 24 h. The obtained material was then dried at 80 °C for 5 h and calcined under an air flow at 500 °C with a heating ramp of 100 °C/h and kept at that temperature for 5 h. The obtained catalyst is denoted as $9-0.554Fe/MOR_{IWI}$.

For the $FeCl_3$ sublimation method [21], the catalyst was prepared through the chemical vapor deposition method using $FeCl_3 \cdot 6H_2O$ as the iron precursor. Briefly, 100 mg of NH_4-MOR and 50 mg of $FeCl_3 \cdot 6H_2O$ reagents were placed at both ends of a porcelain boat. It was then placed in a tube furnace, making $FeCl_3 \cdot 6H_2O$ end on the upstream side in the flowing N_2. Subsequently, the reactor was heated up to 300 °C at a rate of 2 °C/min and kept at that temperature for 3 h, followed by increasing the temperature to 600 °C at a rate of 5 °C/min and maintaining that temperature for 3 h under N_2 flow. Afterward,

the sample was washed with acetone, deionized water, and acetone sequence and dried at 80 °C for 5 h. The catalyst is denoted as 10−0.229Fe/MOR_{subl}.

2.1.2. Different Calcination Temperatures

The commercial NH_4−MOR (n−Si/Al = 9) catalyst was activated before the catalytic reaction, typically by calcination at different temperatures under an air flow with a heating ramp of 100 °C/h, keeping it at that temperature for 5 h. Previous studies [22,23] revealed that high−temperature (>400 °C) pretreatment of ZSM−5 was necessary to acquire high activity. Therefore, prepared catalysts are denoted as MOR(NH_4) (without the activation procedure), MOR(NH_4)−500, MOR(NH_4)−700, and MOR(NH_4)−900, respectively, with regard to their corresponding calcination temperatures of 500 °C, 700 °C, and 900 °C.

In addition to the parent NH_4−MOR (n−Si/Al = 9), Fe−loaded 0.350Fe/MOR$(NH_4)_{mIE}$ catalyst obtained by the modified liquid ion−exchange method with $Fe(acac)_3$ as the precursor was also used to investigate the influence of calcination temperature on the products. The samples were calcined at 500 °C or 700 °C under an air flow with a heating ramp of 100 °C/h and kept at that temperature for 5 h, referred to as 0.350Fe/MOR$(NH_4)_{mIE}$−500 and 0.350Fe/MOR$(NH_4)_{mIE}$−700.

2.1.3. MOR with Different Counter Cations

NH_4−MOR (n−Si/Al = 9, Alfa Aesar), H−MOR (n−Si/Al = 12, ZEOCAT FM−8/25 H), and Na−MOR (n−Si/Al = 6, ZEOCAT FM−8) catalysts with similar Si/Al molar ratios were commercially purchased. Fe was loaded using the modified liquid ion−exchange (mIE) method with $Fe(acac)_3$ as the precursor corresponding to a nominal 0.5 wt.% Fe content (6.3 mg $Fe(acac)_3$), as described in Section 2.1.1. The obtained catalysts are denoted as 0.260Fe/MOR$(NH_4)_{mIE}$, 0.305Fe/MOR$(H)_{mIE}$, and 0.220Fe/MOR$(Na)_{mIE}$.

2.1.4. Different Zeolites Used as Supports

H−ZSM−5 (n−Si/Al = 23, Tricat Inc., Hunt Valley, MD, USA), H−Y (n−Si/Al = 2.6, Alfa Aesar), and H−SAPO−34 (n−Al/P/Si = 1/0.93/0.1, Catalyst Plant of Nankai University, Tianjin, China) catalysts were commercially purchased. Fe was loaded using the modified liquid ion exchange (mIE) method with $Fe(acac)_3$ as the precursor corresponding to a nominal 0.5 wt.% Fe content (6.3 mg $Fe(acac)_3$), as described in Section 2.1.1. The obtained catalysts are denoted as 0.240Fe/ZSM−5$(H)_{mIE}$, 0.470Fe/Y$(H)_{mIE}$ and 0.320Fe/SAPO−34$(H)_{mIE}$.

2.1.5. Different Metal Species

Commercial H−MOR (n−Si/Al = 12, ZEOCAT FM−8/25 H) with only 0.003 wt.% Fe impurity was used as the support to load different metals and reduce the interference from the Fe impurity in NH_4−MOR (n−Si/Al = 9, Alfa Aesar). For metal loading, 200 mg of commercial H−MOR powder and a certain amount of $Cu(acac)_2$ (4.1 mg), $Cr(acac)_3$ (6.7 mg), $Co(acac)_2$ (4.4 mg), or $Mn(acac)_2$ (4.6 mg) metal precursors corresponding to a nominal metal loading of 0.5 wt.% were added to a glass vial containing 8 mL of CH_3CN. The obtained catalysts are denoted as xM/MOR$(H)_{mIE}$ (xM represents the actual contents (wt.%) of the different metals). All other steps and the calcination procedure are similar to the procedure described in Section 2.1.1. The catalysts are denoted as 0.460Cu/MOR$(H)_{mIE}$, 0.030Cr/MOR$(H)_{mIE}$, 0.470Co/MOR$(H)_{mIE}$, and 0.360Mn/MOR$(H)_{mIE}$. In addition, 0.088Fe0.089Cu/MOR$(H)_{mIE}$ catalyst was prepared by adding 0.1 wt.% $Fe(acac)_3$ and 0.1 wt.% $Cu(acac)_2$, and 0.156Fe1.430Cu/MOR$(H)_{mIE}$ catalyst was prepared by adding 0.15 wt.% $Fe(acac)_3$ and 2.5 wt.% $Cu(acac)_2$ instead of 0.5 wt.% of one metal precursor.

2.1.6. Different Fe Loading Contents

For different Fe contents, 200 mg of commercial NH_4−MOR (n−Si/Al = 9, Alfa Aesar) powder and a specific amount of $Fe(acac)_3$ corresponding to a nominal 0.1, 0.5, 1.0, 1.5, or 5.0 wt.% Fe loading (1.3 mg, 6.3 mg, 12.6 mg, 18.9 mg, and 63 mg, respec-

tively) were added to 8 mL of MeCN in a glass vial. The other steps and the calcination procedure are the same as the above procedure described in Section 2.1.1. The catalysts are denoted as MOR(NH_4)−500, 0.160Fe/MOR$(NH_4)_{mIE}$, 0.260Fe/MOR$(NH_4)_{mIE}$, 0.350Fe/MOR$(NH_4)_{mIE}$, 0.390Fe/MOR$(NH_4)_{mIE}$, and 0.600Fe/MOR$(NH_4)_{mIE}$.

2.2. Experimental Methods

2.2.1. Catalytic Methane Oxidation Test

The direct methane oxidation reaction was conducted in a 25 mL stainless−steel autoclave reactor from Parr company (Model 4596) equipped with a homemade Teflon liner vessel and a homemade PTFE stirrer. A flow diagram of the experimental setup is shown in Figure S1. The exact gas volume was measured to be 55.25 mL, as shown in Figure S2. The vessel was loaded with an aqueous solution of H_2O_2 (10 mL, 0.5 M) and the desired amount of catalyst (typically 20 mg), purged three times with 30 bar methane to remove residual air, and finally charged with methane gas to 30 bar. The reaction mixture was then heated up to the desired temperature (typically 80 °C) with a slow stirring rate of 200–300 rpm in the beginning, which usually takes around 15 min to reach 80 °C. Once the desired temperature was achieved, the stirring speed was raised to the maximum of 600 rpm, taken as the reaction's starting point. Once the reaction was finished, the vessel was quickly cooled down in an ice−water bath (below 11 °C) in order to condense the products into their liquid state. The resulting solution was filtered and analyzed by a combination of proton nuclear magnetic resonance (^{1}H NMR), high−performance liquid chromatography (HPLC), and titration methods. The gas product was then collected in an aluminum gas bag and analyzed by gas chromatography coupled with flame ionization detection (GC−FID). Finally, the recyclability of the catalyst was studied for four consecutive cycles. The used catalyst was collected after being centrifuged, washed with deionized water 1 time, and dried at 80 °C for 5 h. Then, the sample was tested directly for the next cycle. After the third run, the used catalyst was calcined for regeneration at 500 °C under an air flow with a heating ramp of 100 °C/h and kept at that temperature for 3 h.

2.2.2. Analysis of Products

1. Gas−phase analysis

The gaseous products were analyzed by gas chromatography (GC, Agilent 7890A) equipped with PLOT&MOLESIEVE columns, a thermal conductivity detector (TCD), and a flame ionization detector (FID), using He as carrier gas. The gaseous products, CH_4, O_2, CO, and CO_2, were quantified against a calibration curve created from commercial standards. An illustrative spectrum is provided in Figure S3.

2. Liquid−phase analysis

The liquid−phase products were analyzed and quantified by ^{1}H NMR on a 400 MHz Bruker AVANCE III nuclear magnetic resonance (NMR) spectrometer. ^{1}H NMR spectra were recorded with a $\pi/2$ pulse width of 10 μs, a recycle delay of 5 s, and 20 scans. Typically, 500 μL of the sample and 100 μL of D_2O with TMSP internal standard (0.12 wt.% trimethylsilylpropanoic acid) were placed in an NMR tube together and mixed thoroughly. A solvent suppression program (ZGPR) was run to minimize the signal arising from the solvent H_2O. The oxygenated products identified were methanol (δ = 3.35 ppm, s), methyl hydroperoxide (δ = 3.86 ppm, s), $HOCH_2OOH$ (δ = 5.04 ppm, s), and formic acid (δ = 8.23 ppm, s). An illustrative spectrum is provided in Figure S4. The chemical shift for $HOCH_2OOH$ matches well with that reported by Cui et al. [9].

3. H_2O_2 quantification

Method 1: The amount of H_2O_2 remaining at the end of the reaction was quantified by titration of the aliquots of the final solution against acidified $Ce(SO_4)_2$ solution using a Ferroin indicator.

Method 2: The consumption of H_2O_2 can also be quantified by high−performance liquid chromatography (HPLC, Agilent 1260 Infinity) equipped with a NUCLEOGEL Sugar

810 H column and a RID detector, using 0.5 mM H_2SO_4 as eluent. The concentration can be calculated using a calibration plot.

4. The calculation of the performance indicators
   (1) The selectivity of the product was defined using Equation (1):

$$\text{Selectivity(MeOH)} = \frac{n(\text{MeOH})}{n(\text{MeOH}) + n(\text{MeOOH}) + n(\text{OHCH}_2\text{OOH}) + n(\text{HCOOH}) + n(\text{CO}_2)} \times 100\% \quad (1)$$

where n(MeOH) refers to the molar amount of MeOH in the reactor after the reaction obtained by the NMR test.

   (2) The conversion of H_2O_2 was defined using Equation (2) or Equation (3):

$$\text{Conversion}_{(\text{H}_2\text{O}_2)} = \frac{\text{peak area of H}_2\text{O}_2\text{ of reaction solution after reaction}}{\text{peak area of H}_2\text{O}_2\text{ aqueous solution before reaction}} \times 100\% \quad (2)$$

The peak areas of H_2O_2 before and after the reaction were obtained by HPLC measurements.

$$\text{Conversion}_{(\text{H}_2\text{O}_2)} = \frac{\text{the consumed Ce(SO}_4)_2\text{volume of reaction solution}}{\text{the consumed Ce(SO}_4)_2\text{volume of H}_2\text{O}_2\text{ solution before reaction}} \times 100\% \quad (3)$$

The consumed volume of $Ce(SO_4)_2$ for reaction solution was obtained by titration.

   (3) The utilization ratio of H_2O_2 was defined using Equation (4):

$$\text{Utilization}_{(\text{H}_2\text{O}_2)} = \frac{n(\text{MeOH}) + n(\text{MeOOH}) + 2n(\text{OHCH}_2\text{OOH}) + 3n(\text{HCOOH})}{n(\text{the total consumption of H}_2\text{O}_2)} \times 100\% \quad (4)$$

The consumption of H_2O_2 of the C_1 oxygenates in Equation (4) is based on the reaction in Equation (5):

$$\text{CH}_4 \underset{-2e^-}{\overset{\text{H}_2\text{O}_2}{\rightarrow}} \begin{matrix}\text{CH}_3\text{OH}\\ \text{CH}_3\text{OOH}\end{matrix} \underset{-2e^-}{\overset{\text{H}_2\text{O}_2}{\rightarrow}} \begin{matrix}\text{HCOH}\\ \text{OHCH}_2\text{OOH}\end{matrix} \underset{-2e^-}{\overset{\text{H}_2\text{O}_2}{\rightarrow}} \text{HCOOH} \underset{-2e^-}{\overset{\text{H}_2\text{O}_2}{\rightarrow}} \text{CO}_2 \quad (5)$$

   (4) Turnover frequencies (TOFs) were defined as micromoles of C_1 oxygenates per micromole of iron and hour (h^{-1}), as shown in Equation (6).

$$\text{TOF} = \frac{n(\text{MeOH}) + n(\text{MeOOH}) + n(\text{OHCH}_2\text{OOH}) + n(\text{HCOOH})}{(\text{mass of catalyst (20mg)} \times \text{ mass fraction of Fe(wt.\%)}/56\text{g/mol}) \times \text{ reaction time(0.5h)}} \quad (6)$$

   (5) Reproducibility of the catalytic results
   The important catalysts in our work were tested repeatedly to ensure reproducibility, especially the 0.260Fe/MOR$(NH_4)_{mIE}$ sample. Multiple catalytic experiments using 0.260Fe/MOR$(NH_4)_{mIE}$ sample showed that its activity could maintain a TOF of around 555 ± 8 h^{-1} and a product yield of about 258 ± 5 μmol.

2.3. Characterizations of the Catalysts

X-ray diffractometry (XRD) analysis was carried out on a BrukerD8 Advance diffractometer at an excitation voltage of 35 kV and a current intensity of 40 mA using Cu Kα (λ = 0.154 nm) radiation. Transmission electron microscopy (TEM) images were collected by Philips CM−200 FEG TEM. Details about XRD and TEM can be found in our previous work [11]. The chemical compositions of the catalysts were determined by a Varian optical emission spectrometer Vista−MPX CCD with inductively coupled plasma optical emission spectrometry (ICP−OES). Acid digestion of the zeolite materials was performed as follows: around 20 mg of sample was digested in a mixture of 1 mL of 49 wt.% HF, 2 mL of 36.5 wt.% HCl, 2 mL of 65 wt.% HNO_3, and 8 mL of double−distilled water.

UV−vis DRS of Fe/MOR catalysts were recorded on a Lambda950 spectrometer in diffuse reflectance (DR) mode at room temperature. The baseline was corrected using $BaSO_4$ as a reference. Samples were scanned in the wavelength range of 200 to 800 nm with a 200 nm/min scan rate. The intensity of the UV−vis DRS spectra was presented in

the form of the Kubelka–Munk function. Deconvolution of the UV−vis DRS spectra into sub−bands was performed by applying the GaussAmp Fit in Origin software.

X-ray absorption spectroscopy (XAS), including X-ray absorption near−edge structure (XANES) and extended X-ray absorption fine structure (EXAFS) of the samples at Fe K−edge, were collected at the beamline 1W1B station of the Beijing Synchrotron Radiation Facility (BSRF), China [24]. A double Si(111)−crystal monochromator was used for energy selection. The Fe K−edge XAFS data were recorded in fluorescence mode. Fe foil and Fe_2O_3 were used as references. All spectra were collected under ambient conditions. The Athena software package was used to analyze the data [25,26].

3. Results and Discussion

The presence of disparate Fe species, such as mononuclear species, oligonuclear clusters, and metal oxide particles, has been experimentally confirmed in Fe−containing zeolites [27,28], in which the majority of Fe species are present as spectator species with limited activity for low−temperature methane oxidation [22,29,30]. Zhu et al. [30] demonstrated that the loading of Fe in a Fe/ZSM−5 catalyst dropped from 2.6 wt.% to 0.03 wt.%, and the yield of the C_1 liquid oxygenates was almost unchanged. According to the literature, the formation of Fe species in zeolites is sensitively dependent on multiple factors, including the preparation route [31], Fe content [30], Fe precursors [32], and calcination temperature [33]. Therefore, we initially prepared Fe/MOR catalysts using four different synthesis procedures, as described in Section 2.1.1, namely, liquid ion exchange (IE), solid−state ion exchange (SSIE), incipient wetness impregnation (IWI), and sublimation of $FeCl_3$ (subl). The corresponding solvent and iron precursors were also considered during the preparation of Fe/MOR catalysts with a nominal content of 0.5 wt.% Fe. Figure 1 shows the performance of the Fe/MOR catalyst in the direct methane oxidation reaction in a batch system under 30 bar of CH_4 and 10 mL of 0.5 M H_2O_2 aqueous solution at 80 °C for 0.5 h. The complete C_1 oxygenate distribution is shown in Table S3. Obviously, compared with the IE, SSIE, and IWI methods, the $FeCl_3$ sublimation method (10−0.229Fe/MOR_{subl} in Figure 1) showed much lower productivity and H_2O_2 utilization ratio and higher CO_2 selectivity. In Figure 1, one can clearly see that Fe/MOR catalysts obtained by the other three typical Fe loading methods all gave excellent yields of C_1 oxygenates of around 250 μmol under suitable conditions, which proved the excellent performance of the MOR zeolite as the Fe support for direct methane oxidation using H_2O_2 as the oxidant. Notably, 1−0.260Fe/MOR$(NH_4)_{mIE}$ (entry 1 in Figure 1), synthesized by using $Fe(acac)_3$ as the precursor and MeCN as the solvent in the liquid ion−exchange process, exhibited a TOF of 555 h^{-1}, significantly exceeding TOFs obtained using all other preparation methods. This highlights the influence of the preparation method on the activity and the high potential of the MOR−based catalyst in direct methane oxidation.

The effect of the choice of Fe precursors in the modified liquid ion−exchange (mIE) method was further examined for the samples obtained by using $Fe(acac)_3$, $Fe(NO_3)_3{\cdot}9H_2O$, and $FeCl_3{\cdot}6H_2O$ (entries 1–3 in Figure 1, respectively). UV−vis DRS was also used to investigate the nature of the Fe(III) species in the catalysts, as depicted in Figure 2. Deconvolution of the absorbance spectra into sub−bands was performed based on the assignments described as follows: UV−vis DRS of Fe−containing zeolites can be divided into three regions: <300 nm, 300–400 nm, and >400 nm, which correspond to the isolated mononuclear Fe^{3+} species with different coordination, oligomeric Fe_xO_y clusters, and Fe_2O_3 nanoparticles, respectively [34,35]. Nevertheless, UV−vis analysis provides a semi−quantitative distribution of these species rather than precise quantities. Although they are of the same order of magnitude [22,36], the relative percentage of the various Fe species does not account for the dependence of the molar extinction coefficient on the wavelength. The Fe distribution listed in Table 1 shows that for the 1−0.260Fe/MOR_{mIE} sample prepared by modified liquid ion exchange with $Fe(acac)_3$ in MeCN, around 98.7% of the iron was present as mononuclear sites of different coordination. As for the samples prepared from $Fe(NO_3)_3{\cdot}9H_2O$ and $FeCl_3{\cdot}6H_2O$ in MeCN, additional spectral features in the >300 nm regions appear

and develop, attributed to the presence of more oligomeric Fe clusters and particles. It is clearly observed that the Fe precursors used during the synthesis determine the nature and proportion of Fe species, which will affect the catalytic performance. Thus, we propose that the advantage of ion exchange with $Fe(acac)_3$ consists of the suppressed Fe aggregation in acetonitrile, achieving more controlled loading with mononuclear Fe species, which may be due to the capping effect of acetylacetonate counter ions. Solomon and coworkers [37] also reported the preparation of Fe−loaded zeolites by diffusion impregnation of $Fe(acac)_3$ in toluene solution to obtain a lower iron content (0.3 wt%), which minimized Fe heterogeneity and limited the formation of oxide/hydroxide species (relative to aqueous exchange or sublimation). These findings provide valuable insights for the design of highly efficient Fe/MOR catalysts for the activation of methane. Adopting MeCN as the solvent allows for the suppression of the hydrolysis of $Fe(acac)_3$ to achieve selective loading of mononuclear Fe species.

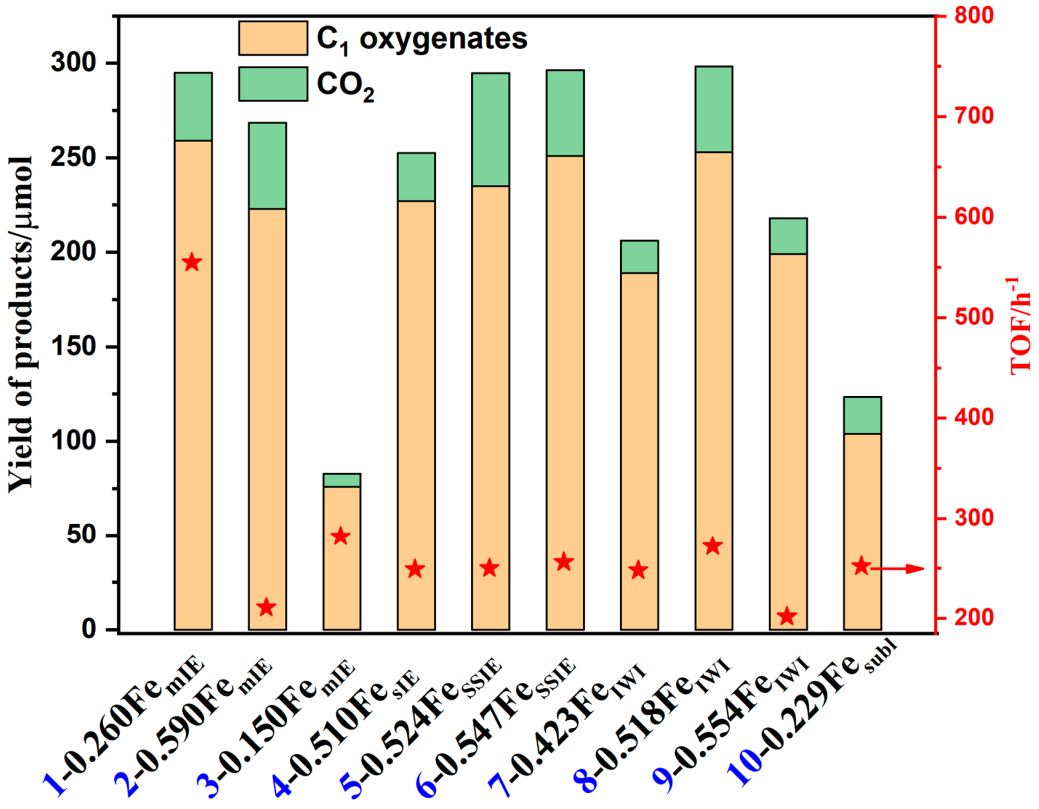

Figure 1. Dependence of performance on synthesis method. Reaction conditions: 30 bar CH_4, 10 mL 0.5 M H_2O_2, 600 rpm, 80 °C, 0.5 h, and 20 mg catalyst. All the catalysts were prepared starting from commercial NH_4−MOR (n−Si/Al = 9) and finally calcined at 500 °C under an air flow with a heating ramp of 100 °C/h and kept at that temperature for 5 h. The product distribution is given in Table S3.

Table 1. Deconvolution data of UV−vis DRS over Fe/MOR_{mIE} catalysts prepared by different iron precursors.

Catalysts	Relative Contribution of Different Range (%) [a]		
	I_1 (200~300 nm)	I_2 (300~400 nm)	I_3 (>400 nm)
1−0.260Fe/MOR_{mIE}	98.7	1.3	0
2−0.590Fe/MOR_{mIE}	72.2	25.4	2.4
3−0.150Fe/MOR_{mIE}	62.7	35.2	2.1

[a] Obtained by using Origin software (GaussAmp Fit), $R^2 > 0.99$.

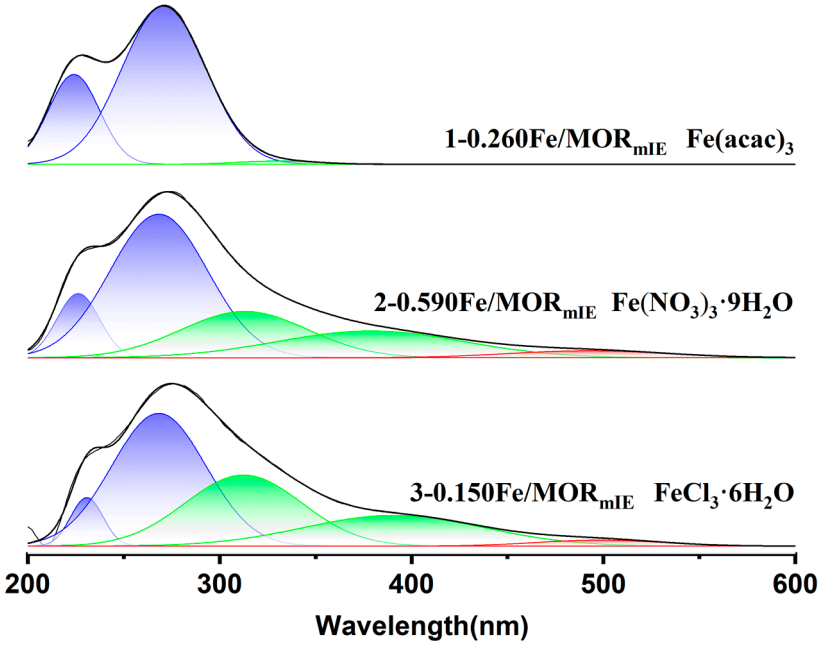

Figure 2. UV−vis DRS of Fe/MOR catalysts for samples (entries 1–3) prepared by the modified liquid ion−exchange method (mIE) in MeCN as the solvent with different iron precursors: $Fe(acac)_3$, $Fe(NO_3)_3 \cdot 9H_2O$, and $FeCl_3 \cdot 6H_2O$, respectively.

After successfully demonstrating that Fe−loaded NH_4−MOR (n−Si/Al = 9) zeolites exhibited good activity using different methods, we focused on the best catalyst, $0.260Fe/MOR(NH_4)_{mIE}$. Further, we analyzed the external factors determining its activity (see Figure 3 and Table S4). By analyzing the composition of the commercial NH_4−MOR, it was found to contain 0.06 wt.% Fe as an impurity, which may cause certain activity [10]. However, the pristine NH_4−MOR did not show significant activity (see 1−MOR in Figure 3). High−temperature calcination at 500 °C in the air significantly increased the activity of commercial NH_4−MOR (see 2−MOR−500 in Figure 3). The heat treatment process contributed to the formation of active Fe sites, which can activate H_2O_2 at 80 °C [22,23]. A reasonable structural evolution could be that the framework Fe species migrate into the channels of the MOR zeolite and form extra−framework Fe species upon calcination, analogous to what was found for Fe/MFI [10,23]. Despite the good activity of the Fe impurity in MOR, loading more highly active Fe sites is essential for increasing the yield.

In addition to ammonium−type MOR, another two commercial MOR catalysts with sodium and hydrogen counter cations were also used as supports in order to load Fe under the same preparation conditions (mIE) and test the activity shown in Figure 3 and Table S4. As seen in entry 3, the product yield was significantly reduced by using $0.220Fe/MOR(Na)_{mIE}$. NH_4^+−type zeolites can transform to the H−form after high−temperature calcination. Both $0.305Fe/MOR(H)_{mIE}$ (entry 4) and $0.260Fe/MOR(NH_4)_{mIE}$ (entry 5) exhibited good activity, with TOFs of 527 and 555 h^{-1}, which implies the significance of Brønsted acid sites [23,38]. The $0.260Fe/MOR(NH_4)_{mIE}$ sample was selected as a model catalyst for its superior performance (entry 6 to entry 9). In entry 6, a blank experiment is shown, i.e., only H_2O_2 without the addition of the solid catalyst, which shows only trace activity (9.2 μmol), indicating the decisive role of the solid catalyst. The presence of the trace activity can be ascribed to the self−decomposition of H_2O_2 at 80 °C. In entry 7, there were no C_1 oxygenates generated after replacing CH_4 with N_2, which verifies that all of the carbon products originate from CH_4. Another aspect, the high consumption of H_2O_2 under a N_2 atmosphere, implies that the CH_4 atmosphere plays a positive role in suppressing the self−decomposition of H_2O_2. Hammond et al. [39] also verified that the presence of methane could be beneficial to the stability of the products, potentially by competitively adsorbing onto the active sites. The competitive adsorption of CH_4 molecules on Fe sites was supposed to inhibit the decompo-

sition of H_2O_2. In entry 8, there were no products detected in the reaction solution without the addition of H_2O_2, suggesting that using H_2O_2 solution as the oxidant is essential for the reaction. In entry 9, the reaction was conducted over the 0.260Fe/MOR$(NH_4)_{mIE}$ catalyst at a low temperature of 50 °C for 1 h, giving smaller product yields than the result in entry 5 at 80 °C, which confirms the selection of 80 °C as the reaction temperature. Therefore, all of these factors, high−temperature treatment, Brønsted acid sites, CH_4, H_2O_2, and 80 °C reaction temperature, determine the catalytic performance of 0.260Fe/MOR$(NH_4)_{mIE}$. After a 10 min reaction, the suspension was collected for the hot−filtration experiment (see entry 10 in Table S4). It turns out that this suspension barely exhibits the conversion of methane (see entry 11 in Table S4). At the same time, the original C_1 products were oxidized to CO_2 by hot H_2O_2. In addition, the 0.290Fe/MOR$(H)_{mIE}$ catalyst was tested for its recyclability in four consecutive runs (Table S5 and Figure S5). The activity can be easily regenerated in the fourth run after a simple calcination treatment. A higher degree of over−oxidation in the fourth run is probably because the repeated calcination resulted in the aggregation of the Fe species. The slight decrease in activity in the third run should be due to the accumulated carbonaceous species adsorbed on the catalyst surface [30]. The supernatant of the first and third runs was subjected to ICP measurement to check the leaching of Fe. It could only detect a trace amount of Fe, corresponding to 0.12 at% based on the total amount of Fe in the applied catalyst (20 mg). Such a trace amount of leached Fe could be from the trace Fe residue from the precursor or the reactor itself. The good retention of Fe in the catalyst could prove the heterogeneity of the Fe/MOR_{mIE} catalyst.

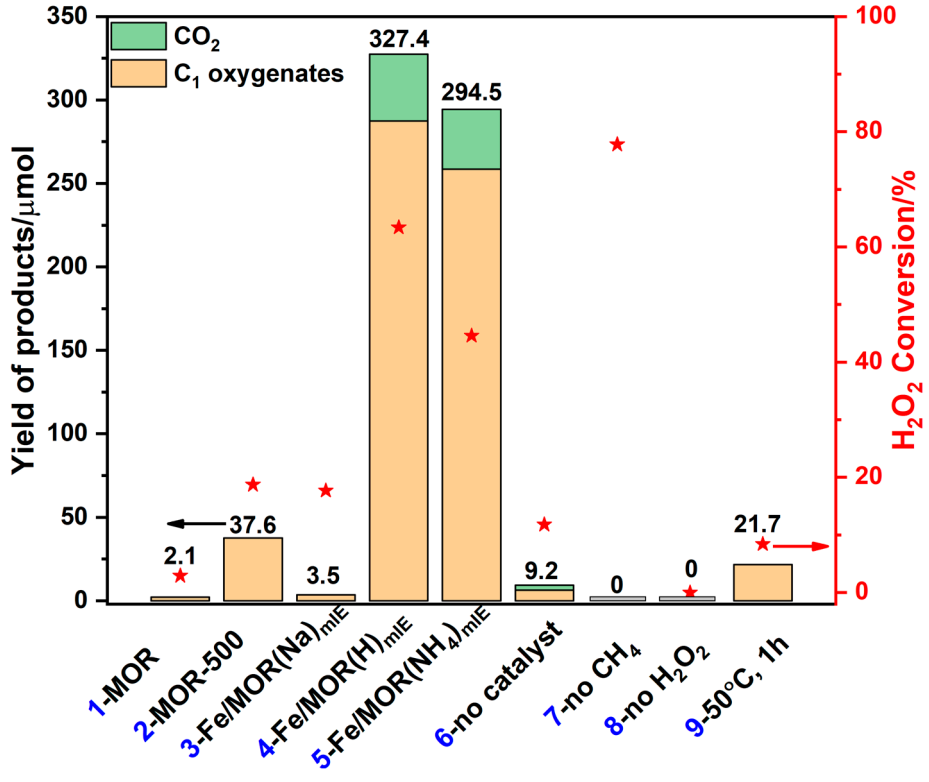

Figure 3. Catalytic performance for direct methane oxidation over 0.260Fe/MOR$(NH_4)_{mIE}$ catalyst prepared from $Fe(acac)_3$ in MeCN solution via liquid ion−exchange method. Reaction conditions: 30 bar CH_4, 10 mL 0.5 M H_2O_2, 600 rpm, 80 °C, 0.5 h, and 20 mg catalyst. Entry 6: without solid catalyst; Entry 7: replacing CH_4 with 30 bar of N_2; Entry 8: replacing H_2O_2 aqueous solution with 10 mL H_2O; Entry 9: employing 50 °C and 1 h as reaction temperature and time. The product distribution is given in Table S4.

The effect of the calcination temperature is further investigated and discussed in Table S6. The catalytic activity of the commercial NH_4-MOR sample in the direct methane oxidation reaction was shown to be strongly dependent on the calcination temperature (Figure 3). Thus, when increasing the calcination temperature to 700 °C (entry 3, Table S6), the TOF value was increased significantly from 352 h^{-1} to 1633 h^{-1}. When further increasing it up to 900 °C (entry 4, Table S6), the TOF value of MOR−900 (1315 h^{-1}) did not change correspondingly but caused much higher CO_2 generation and a lower H_2O_2 utilization ratio. As we know, a very high calcination temperature can lead to the aggregation of the iron species, resulting in a weakened catalytic performance for direct methane oxidation [22]. This principle applies to the Fe impurity in commercial NH_4-MOR. The XRD patterns of MOR(NH_4) after calcination at different temperatures are given in Figure S6. There is a decrease in crystallinity for MOR−900, but the complete crystalline structure is still maintained. As for the exogenous Fe species, the 0.350Fe/MOR$(NH_4)_{mIE}$ catalyst prepared by the modified ion−exchange method was taken as an example, which was calcined at 500 °C (entry 5, Table S6) and 700 °C (entry 6, Table S6). After increasing the calcination temperature to 700 °C for Fe/MOR, more H_2O_2 decomposition, lower catalytic activity (TOF), and higher CO_2 yield can be observed, indicating serious over−oxidation after calcination at a temperature higher than 500 °C. Compared with the pristine MOR sample, Fe/MOR is more sensitive to the temperature, possibly due to easier aggregation at higher loading.

Different topologies and compositions of Fe−modified zeolites are believed to have an enormous impact on the nature and distribution of the Fe species and the ability to generate C_1 products. In addition to H−MOR, other classic commercial zeolites, namely, H−ZSM−5, H−Y, and H−SAPO−34, were used to load Fe with the same modified liquid ion−exchange method with a nominal Fe content of 0.5 wt.%. Figure 4 and Table S7 show the catalytic performance of various Fe−loaded zeolites in direct methane oxidation. Fe/ZSM−5 has received intensive research in the last decade for its excellent activity in direct methane oxidation at 50 °C to 80 °C when using an H_2O_2 aqueous solution [10,30]. As expected, the as−prepared 0.240Fe/ZSM−5$(H)_{mIE}$ catalyst exhibited good activity with 747 h^{-1} TOF to C_1 oxygenates and produced almost equal amounts of oxygenates and CO_2. Despite not being as active as Fe/ZSM−5 zeolites, Fe/MOR is a real alternative and can be used for fundamental studies on catalytically relevant active sites for direct methane oxidation. The 0.305Fe/MOR$(H)_{mIE}$ catalyst showed a C_1 oxygenate yield similar to that of 0.240Fe/ZSM−5$(H)_{mIE}$ with less CO_2 formation. Besides ZSM−5 and MOR zeolites, SAPO−34 and Y were loaded with Fe but did not show significant activities. Furthermore, various kinds of metals, such as Cu, Cr, Co, and Mn, were screened for the oxidation reaction of methane, of which Fe/MOR showed the highest activity. Considering H_2O_2 conversion, all M/MORs (M = Cu, Cr, Co, and Mn) can activate H_2O_2 without producing significant C_1 products, which results in a relatively low H_2O_2 utilization ratio (Figure 4). These results indicate that methane oxidation using H_2O_2 strongly depends on the nature of the metal species and the zeolite support. Therefore, the presence of Fe species in MOR was crucial for substantial catalytic activities.

It was reported that the addition of Cu to the reaction in different forms, such as a co−component of the catalyst, as a solid catalyst in a physical mixture, or Cu^{2+} ions in the reaction solution, could suppress the over−oxidation of methanol and improve the methanol selectivity. The proposed reason behind this phenomenon was that the presence of Cu could decrease the concentration of active species hydroxyl radicals (•OH) to inhibit the further oxidation of methanol [10,29]. As shown in Table S8 and Figure S7, besides Cu, MOR(H) loaded with/without different metal species were physically mixed and added as modulators to investigate their influence on the selectivity over the 0.260Fe/MOR$(NH_4)_{mIE}$ catalyst. The yield of HCOOH and CO_2 apparently decreased with similar amounts of CH_3OH and CH_3OOH after adding these additives, indicating suppressed over−oxidation. This result is also consistent with the proposed reaction scheme in the literature [9,19] that CH_4 was first oxidized to CH_3OOH and CH_3OH. Then, CH_3OH was further converted

into $HOCH_2OOH$ and consecutively oxidized by •OH into HCOOH and CO_2 (Figure S8). Therefore, it is first proposed that apart from Cu, these variable−valence metal species can also scavenge •OH radicals to suppress over−oxidation, resulting in the decreased yield of HCOOH and CO_2. Furthermore, as shown in Figure S7, when Cu was added as a co−component to prepare FeCu/MOR(H) catalysts, $0.088Fe0.089Cu/MOR(H)_{mIE}$ and $0.156Fe1.430Cu/MOR(H)_{mIE}$ catalysts exhibited similar TOFs in CH_3OH and CH_3OOH to that of the physically mixed catalyst $0.260Fe/MOR(NH_4)_{mIE}$ + $0.460Cu/MOR(H)_{mIE}$. This result indicates that the form of Cu present in the reaction did not strongly influence its effect.

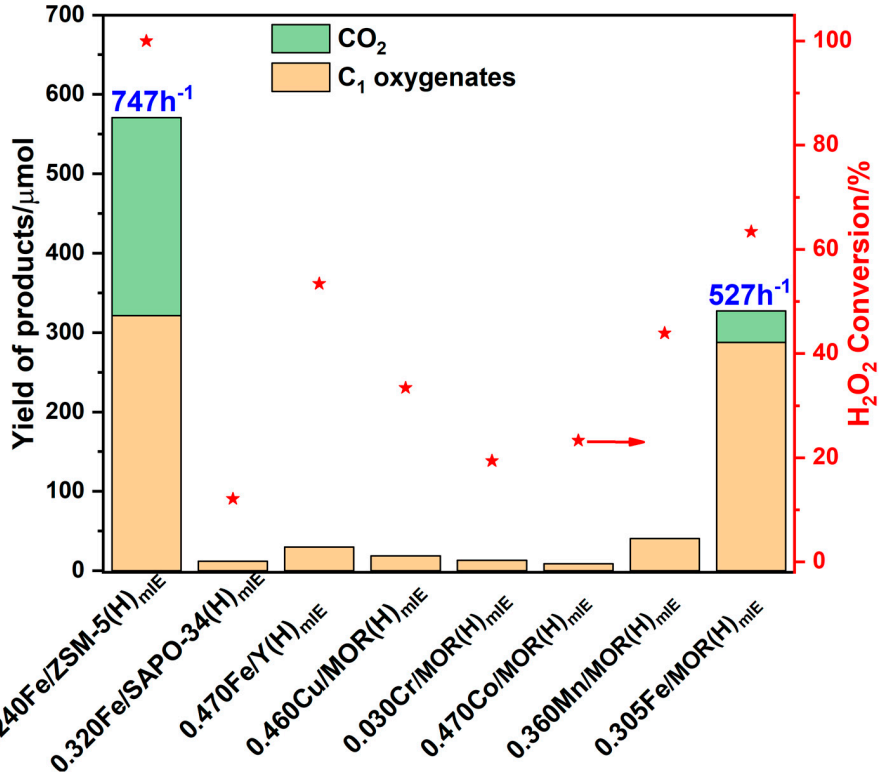

Figure 4. Catalytic performance of different Fe−modified zeolites and MOR(H) catalysts modified with different metals in the direct methane oxidation. Reaction conditions: 30 bar CH_4, 10 mL 0.5 M H_2O_2, 600 rpm, 80 °C, 0.5 h, and 20 mg catalyst. Commercial MOR(H) with an n−Si/Al ratio of 12 was used as support due to negligible Fe impurity. The product distribution is given in Table S7.

In order to determine the optimum loading with the underlying structure–performance relation, different Fe contents were investigated on $Fe/MOR(NH_4)_{mIE}$ catalysts. Thus, the catalysts were obtained by increasing the $Fe(acac)_3$ precursor concentration corresponding to nominal loadings of 0, 0.1, 0.5, 1.0, 1.5, and 5.0 wt.% Fe. Despite the increasing amount of Fe precursor, the actual Fe loading did not increase proportionally (see Figure S9), probably due to a diffusion limitation of $Fe(acac)_3$ inside the pores of MOR. Previous work [37] utilized this diffusion effect to controllably achieve a low iron content (0.3 wt%) with the predominance of mononuclear α−Fe(ii) sites in Fe/ZSM−5. The catalytic performance was evaluated by monitoring the product yield and TOF of Fe/MOR catalysts with a series of Fe loadings. Figure 5 shows that around 0.260 wt.% Fe was the optimal loading, which exhibited the best yield of 259 μmol C_1 oxygenates and a maximum TOF of 555 h^{-1}. Catalysts with 0.350 wt.% and 0.390 wt.% Fe possessed similar C_1 yields and H_2O_2 utilization ratios to their 0.260 wt.% counterpart, but with increasing HCOOH and CO_2 selectivity and decreasing TOFs (Figure 5 and Table S9). As for $0.600Fe/MOR(NH_4)_{mIE}$, a significant drop in the H_2O_2 utilization ratio and TOF with obviously increasing CO_2 yield is probably explained by the presence of different Fe species that tend to trigger undesired

side−reactions (H_2O_2 decomposition and over−oxidation). There is a plateau in the yield of C_1 oxygenates from 0.260 to 0.600 wt.% of Fe/MOR catalysts, which may be because CH_4 diffusion into Fe active sites in MOR is restricted in the batch reactor system. Spectroscopic studies were conducted to distinguish the Fe species (see Figure 6 and Table 2). UV−vis DRS showed that 98.7% of the iron at 0.260 wt.% content was present as mononuclear sites of different coordination. By further increasing the Fe content, significant aggregation can be observed due to a higher proportion of oligomeric clusters and even the appearance of Fe_2O_3 nanoparticles for the 0.600 wt.% Fe sample, which fits the catalytic results. By comparing the TOFs with the fraction of Fe sites determined from UV−vis DRS, the TOFs were observed to drop with the decreasing fraction of monomeric Fe, which can be assumed to indicate that monomers are the active sites for direct methane oxidation in Fe/MOR (see Figure S10) [19].

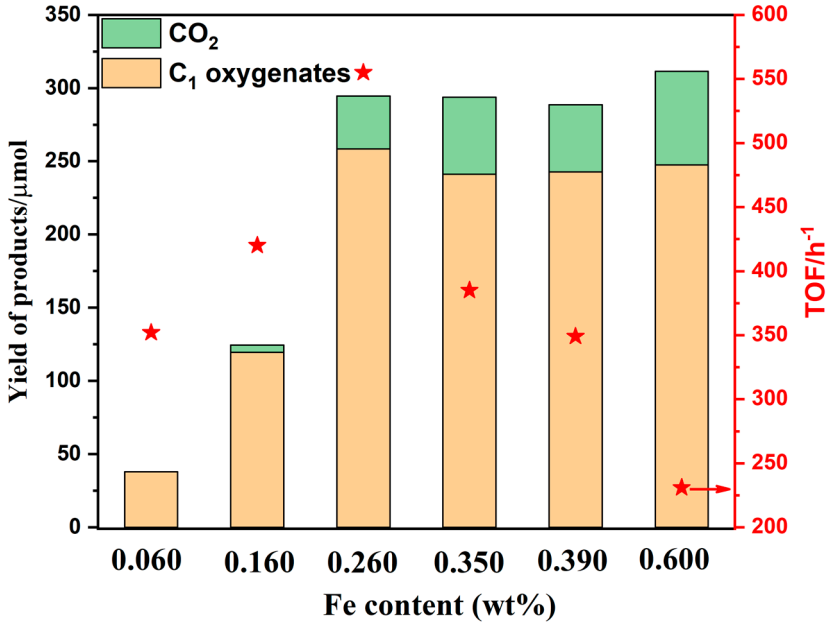

Figure 5. Catalytic performance of Fe/MOR$(NH_4)_{mIE}$ catalysts with different Fe loadings prepared from $Fe(acac)_3$ in MeCN solution via liquid ion−exchange method. Reaction conditions: 30 bar CH_4, 10 mL 0.5 M H_2O_2, 600 rpm, 80 °C, 0.5 h, and 20 mg catalyst. Commercial MOR(NH_4) with an n−Si/Al ratio of 9 containing 0.06 wt.% Fe impurity was used as support. The product distribution is given in Table S9.

Table 2. Deconvolution data of UV−vis DRS over Fe/MOR_{mIE} catalysts with different Fe loadings.

Catalysts	Relative Contribution of Different Ranges (%) [a]		
	I_1 (200~300 nm)	I_2 (300~400 nm)	I_3 (>400 nm)
0.260Fe/MOR$(NH_4)_{mIE}$	98.7	1.3	0
0.305Fe/MOR$(H)_{mIE}$	95.2	4.8	0
0.350Fe/MOR$(NH_4)_{mIE}$	92.6	7.4	0
0.600Fe/MOR$(NH_4)_{mIE}$	83.4	11.4	5.2

[a] Obtained by using Origin software (GaussAmp Fit), $R^2 > 0.99$.

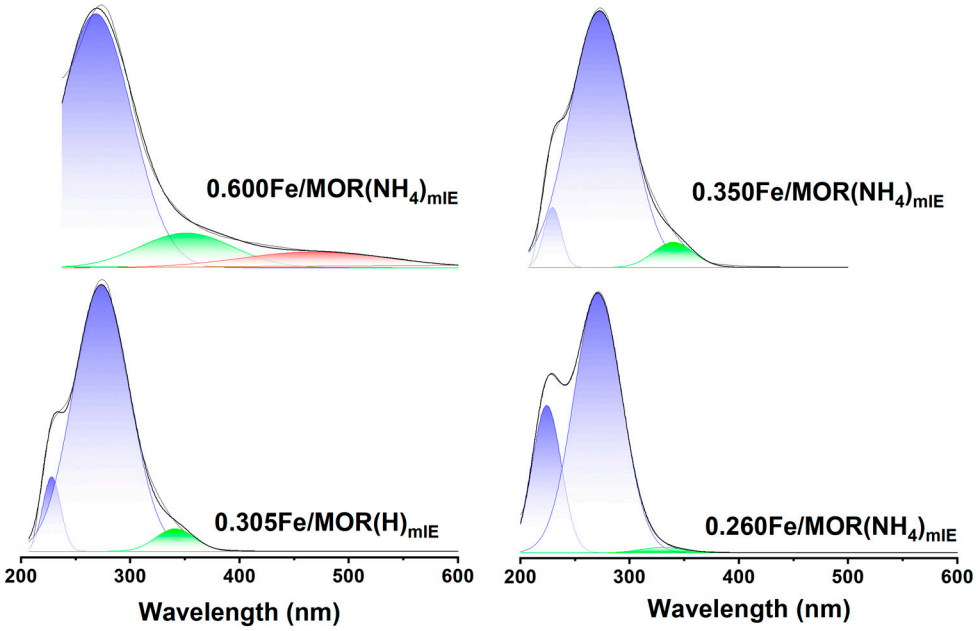

Figure 6. UV−vis DRS of Fe/MOR_{mIE} catalysts prepared by modified liquid ion−exchange method with different Fe contents. Except for 0.305Fe/$MOR(H)_{mIE}$, other catalysts were obtained using NH_4−MOR as support.

Further characterizations were also applied to determine the specific state of Fe species in MOR. Accordingly, the TEM image failed to distinguish apparent Fe−based nanoparticles, indicating the existence of sub−nanometer Fe species in MOR below the detection limit of TEM (Figure 7a). To further investigate the coordination environment of Fe in MOR zeolites, X-ray absorption spectroscopy (XAS) was performed. According to the X-ray absorption near−edge structure (XANES) spectrum of the Fe K−edge, the energy absorption threshold of Fe/MOR was located slightly lower than that of Fe_2O_3, suggesting a little reduced Fe(III) in Fe/MOR (Figure 7b). The Fourier transform−extended X-ray absorption fine structure (FT−EXAFS) spectrum shows two dominating peaks below 2 Å, which can be ascribed to two kinds of Fe−O scattering paths (Figure 7c). There are no apparent observations of the Fe−Fe scattering path (Fe foil (2.21 Å), Fe_2O_3 (2.56 Å)), confirming the absence of Fe−Fe bonds and atomic dispersion of Fe sites in 0.350Fe/$MOR(NH_4)_{mIE}$. The fitting of FT−EXAFS was further conducted to determine the coordination environments (Figures 7d and S11). The best fit was achieved by FeO_6 coordination with two types of Fe−O bonds, excluding the existence of binuclear clusters, trinuclear clusters, and Fe_2O_3 (Figure S12). The bond lengths of 1.85 and 2.04 Å correspond to Fe−O−Al/Si and Fe−OH/H_2O, respectively [40,41]. The corresponding fitting parameters are summarized in Table S10. In addition, the wavelet−transformed (WT) EXAFS spectrum also indicates the atomic state of Fe species in MOR (Figure 7e), which gives a more descriptive evaluation.

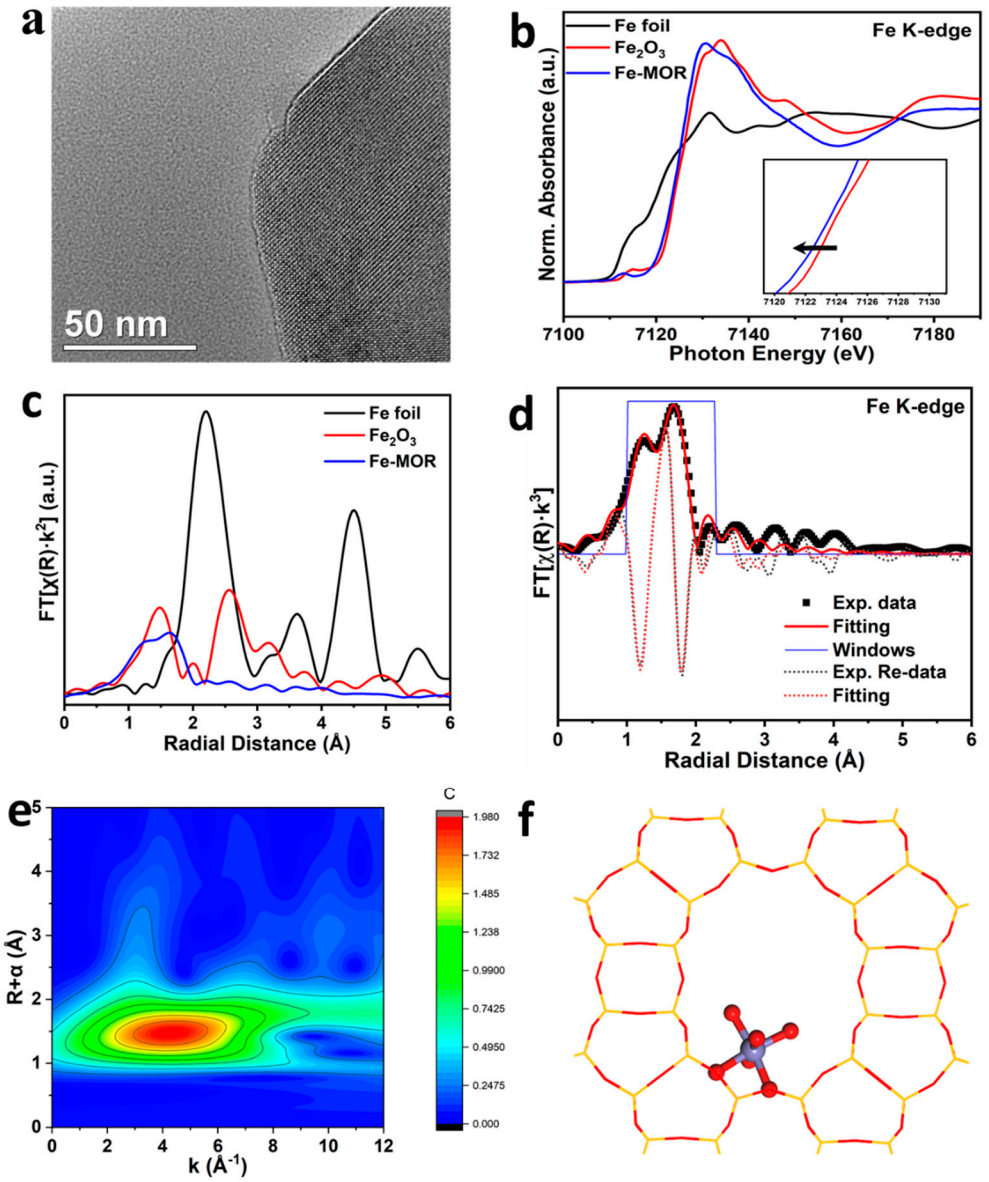

Figure 7. TEM image and XAS analysis of 0.350Fe/MOR$(NH_4)_{mIE}$. (**a**) TEM image. (**b**) Fe K−edge XANES spectra and (**c**) FT−EXAFS spectra of 0.350Fe/MOR$(NH_4)_{mIE}$, Fe foil, and Fe_2O_3. (**d**) EXAFS fitting in R−space and (**e**) WT−EXAFS of 0.350Fe/MOR$(NH_4)_{mIE}$. (**f**) The proposed structure of mononuclear Fe in MOR, viewing along the c-axis. Pink: Al; Yellow, Si; Red: O; Purple: Fe.

4. Conclusions

A modified liquid ion−exchange method was used in this work to control Fe loading in MOR−type zeolites. The loading procedure was conducted using $Fe(acac)_3$ with 0.5 wt.% Fe as the precursor in CH_3CN solution to obtain around 0.30 wt.% Fe content due to the diffusion effect. The obtained 0.260Fe/MOR_{mIE} catalyst exhibited excellent catalytic performance with a record TOF value of 555 h^{-1} in the direct methane oxidation reaction in a batch reactor using H_2O_2 as the oxidant. By comparing the catalytic performance with the concentration of Fe sites, as determined from spectroscopic studies, it was proved that the mononuclear Fe ions are assumed as the active sites, which was also verified by XAS and UV−vis DRS. In contrast to aqueous exchange or sublimation, the advantage of this method was proposed to be the minimized Fe heterogeneity and the limited formation of oxide species to controllably achieve the predominance of mononuclear Fe sites in MOR. Unlike the previously proposed binuclear Fe as active sites in MOR, these new findings

expand our understanding of the intrinsic active site for direct methane oxidation in the Fe/H_2O_2−mediated system.

Supplementary Materials: The following supporting information can be downloaded at: https://www.mdpi.com/xxx/s1. Table S1: The representative catalysts of low-temperature methane oxidation with H_2O_2 as oxidant; Table S2: The source and purity of the chemicals mentioned in the text; Table S3: Catalytic performances of $Fe/MOR(NH_4)$ catalysts prepared by different methods; Table S4: Catalytic studies of Fe/MOR_{mIE} catalysts prepared by modified liquid ion exchange method with $Fe(acac)_3$ as the precursor in MeCN; Table S5: Reaction tests for the recycle and regeneration of the $0.290Fe/MOR(H)_{mIE}$ catalyst; Table S6: The effect of heat-treatment temperature on the performance of the $0.350Fe/MOR(NH_4)_{mIE}$ and parent $MOR(NH_4)$ with Fe impurity; Table S7: Catalyst performance of MOR(H) and other zeolites loaded with different metals by the modified liquid ion exchange method; Table S8: Addition of a second metal to suppress the over-oxidation in direct methane oxidation with Fe/MOR_{mIE}; Table S9: Performance of $Fe/MOR(NH_4)_{mIE}$ with different Fe loadings; Table S10: EXAFS fitting parameters of Fe/MOR, using different modes. Figure S1: The flow diagram of the experimental setup in this work; Figure S2: (a) Schematic diagram of the U-type gas measuring device; (b) Formula for the calculation of the reactor's gas volume V_0; Figure S3: Example of the gaseous products quantification by GC; Figure S4: Example of the product quantification by ^1H NMR with solvent suppression program; Figure S5: Reaction tests for the recycle and regeneration of the $0.290Fe/MOR(H)_{mIE}$ catalyst; Figure S6: The XRD patterns of $MOR(NH_4)$-500, $MOR(NH_4)$-700 and $MOR(NH_4)$-900; Figure S7: Catalytic studies of the addition of a second metal by physical mixture or as a co-component on the catalyst to suppress the over-oxidation by Fe/MOR in direct methane oxidation. Reaction conditions: 30 bar CH_4, 10 mL 0.5 M H_2O_2, 600 rpm, 80 °C, 0.5 h, 20 mg catalyst and/or 20 mg of co-catalyst. All the catalysts used during the reaction were calcined under the air flow at 500 °C with a heating ramp of 100 °C/h and kept at that temperature for 5 h; Figure S8: Proposed reaction scheme for direct methane oxidation in the H_2O_2-based heterogeneous system; Figure S9: The loading effect of $Fe(acac)_3$ precursor on commercial NH_4-MOR zeolite containing 0.06 wt.% Fe impurity in CH_3CN solution. The complete loading procedure is described in 2.1.6 in the text; Figure S10: The relative proportion of different Fe species in Fe/MOR_{mIE} zeolites with the TOFs to C_1 oxygenates; Figure S11: EXAFS fitting in k-space; Figure S12: Potential Fe structures hosted in MOR zeolite considered in XAS fitting. (a) single atom Fe in 12 MR. (b) binuclear Fe in 6 MR. (c) trinuclear Fe in 8 MR. (d) α-Fe_2O_3. Pink: Al; Yellow, Si; Red: O; Purple: Fe.

Author Contributions: Conceptualization, C.X. and E.K.; methodology, C.X.; software, H.L.; validation, C.X.; formal analysis, C.X.; investigation, C.X.; resources, E.K., N.M. and Q.S.; data curation, C.X.; writing—original draft preparation, C.X.; writing—review and editing, C.X. and E.K.; visualization, C.X.; supervision, E.K.; project administration, E.K.; funding acquisition, E.K. All authors have read and agreed to the published version of the manuscript.

Funding: This research was funded by China Scholarship Council, grant number 201806340103.

Institutional Review Board Statement: Not applicable.

Informed Consent Statement: Not applicable.

Data Availability Statement: Not applicable.

Acknowledgments: We are grateful to the Beijing Synchrotron Radiation Laboratory (BSRF) for access to X-ray absorption spectroscopy (XAS) measurements. We are appreciative to Instituts für Organische Chemie (IOC) for the NMR tests. We greatly thank Yvonne Traa and M. Eng. Faeze Tari for proofreading the manuscript.

Conflicts of Interest: The authors declare no conflict of interest.

References

1. Arndtsen, B.A.; Bergman, R.G.; Mobley, T.A.; Peterson, T.H. Selective Intermolecular Carbon−Hydrogen Bond Activation by Synthetic Metal Complexes in Homogeneous Solution. *Accounts Chem. Res.* **1995**, *28*, 154–162. [CrossRef]
2. Dinh, K.T.; Sullivan, M.M.; Serna, P.; Meyer, R.J.; Dincă, M.; Román−Leshkov, Y. Viewpoint on the Partial Oxidation of Methane to Methanol Using Cu− and Fe−Exchanged Zeolites. *ACS Catal.* **2018**, *8*, 8306–8313. [CrossRef]

3. Yuan, S.; Li, Y.; Peng, J.; Questell-Santiago, Y.M.; Akkiraju, K.; Giordano, L.; Zheng, D.J.; Bagi, S.; Román-Leshkov, Y.; Shao-Horn, Y. Conversion of Methane into Liquid Fuels—Bridging Thermal Catalysis with Electrocatalysis. *Adv. Energy Mater.* **2020**, *10*, 2002054. [CrossRef]
4. Sun, L.; Wang, Y.; Guan, N.; Li, L. Methane Activation and Utilization: Current Status and Future Challenges. *Energy Technol.* **2019**, *8*, 1900826. [CrossRef]
5. Snyder, B.E.R.; Bols, M.; Schoonheydt, R.A.; Sels, B.F.; Solomon, E.I. Iron and Copper Active Sites in Zeolites and Their Correlation to Metalloenzymes. *Chem. Rev.* **2018**, *118*, 2718–2768. [CrossRef]
6. Ravi, M.; Ranocchiari, M.; Van Bokhoven, J.A. The Direct Catalytic Oxidation of Methane to Methanol—A Critical Assessment. *Angew. Chem. Int. Ed.* **2017**, *56*, 16464–16483. [CrossRef]
7. Freakley, S.J.; Dimitratos, N.; Willock, D.J.; Taylor, S.H.; Kiely, C.J.; Hutchings, G.J. Methane Oxidation to Methanol in Water. *Acc. Chem. Res.* **2021**, *54*, 2614–2623. [CrossRef]
8. Newton, M.A.; Knorpp, A.J.; Sushkevich, V.L.; Palagin, D.; Van Bokhoven, J.A. Active sites and mechanisms in the direct conversion of methane to methanol using Cu in zeolitic hosts: A critical examination. *Chem. Soc. Rev.* **2020**, *49*, 1449–1486. [CrossRef]
9. Cui, X.; Li, H.; Wang, Y.; Hu, Y.; Hua, L.; Li, H.; Han, X.; Liu, Q.; Yang, F.; He, L.; et al. Room−Temperature Methane Conversion by Graphene−Confined Single Iron Atoms. *Chem* **2018**, *4*, 1902–1910. [CrossRef]
10. Hammond, C.; Forde, M.; Rahim, M.H.A.; Thetford, A.; He, Q.; Jenkins, R.L.; Dimitratos, N.; Lopez−Sanchez, J.A.; Dummer, N.; Murphy, D.; et al. Direct Catalytic Conversion of Methane to Methanol in an Aqueous Medium by using Copper−Promoted Fe−ZSM−5. *Angew. Chem. Int. Ed.* **2012**, *51*, 5129–5133. [CrossRef]
11. Zuo, H.; Xin, Q.; Meynen, V.; Klemm, E. Sensitivity of the selective oxidation of methane over Fe/ZSM−5 zeolites in a micro fixed−bed reactor for the catalyst preparation method. *Appl. Catal. A Gen.* **2018**, *566*, 96–103. [CrossRef]
12. Rahim, M.H.A.; Forde, M.; Jenkins, R.L.; Hammond, C.; He, Q.; Dimitratos, N.; Lopez−Sanchez, J.A.; Carley, A.F.; Taylor, S.; Willock, D.J.; et al. Oxidation of Methane to Methanol with Hydrogen Peroxide Using Supported Gold−Palladium Alloy Nanoparticles. *Angew. Chem. Int. Ed.* **2013**, *52*, 1280–1284. [CrossRef] [PubMed]
13. Kwon, Y.; Kim, T.Y.; Kwon, G.; Yi, J.; Lee, H. Selective Activation of Methane on Single−Atom Catalyst of Rhodium Dispersed on Zirconia for Direct Conversion. *J. Am. Chem. Soc.* **2017**, *139*, 17694–17699. [CrossRef] [PubMed]
14. Bai, S.; Liu, F.; Huang, B.; Li, F.; Lin, H.; Wu, T.; Sun, M.; Wu, J.; Shao, Q.; Xu, Y.; et al. High−efficiency direct methane conversion to oxygenates on a cerium dioxide nanowires supported rhodium single−atom catalyst. *Nat. Commun.* **2020**, *11*, 954. [CrossRef]
15. Zhou, H.; Liu, T.Y.; Zhao, X.Y.; Zhao, Y.F.; Lv, H.W.; Fang, S.; Wang, X.Q.; Zhou, F.Y.; Xu, Q.; Xu, J.; et al. A Supported Nickel Catalyst Stabilized by a Surface Digging Effect for Efficient Methane Oxidation. *Angew. Chem. Int. Ed.* **2019**, *58*, 18388–18393. [CrossRef]
16. Shen, Q.; Cao, C.; Huang, R.; Zhu, L.; Zhou, X.; Zhang, Q.; Gu, L.; Song, W.-G. Single Chromium Atoms Supported on Titanium Dioxide Nanoparticles for Synergic Catalytic Methane Conversion under Mild Conditions. *Angew. Chem. Int. Ed.* **2019**, *59*, 1216–1219. [CrossRef]
17. Osadchii, D.Y.; Olivos−Suarez, A.I.; Szécsényi, Á.; Li, G.; Nasalevich, M.A.; Dugulan, I.A.; Crespo, P.S.; Hensen, E.J.M.; Veber, S.L.; Fedin, M.V.; et al. Isolated Fe Sites in Metal Organic Frameworks Catalyze the Direct Conversion of Methane to Methanol. *ACS Catal.* **2018**, *8*, 5542–5548. [CrossRef]
18. Zhao, W.; Shi, Y.; Jiang, Y.; Zhang, X.; Long, C.; An, P.; Zhu, Y.; Shao, S.; Yan, Z.; Li, G.; et al. Fe-O Clusters Anchored on Nodes of Metal–Organic Frameworks for Direct Methane Oxidation. *Angew. Chem. Int. Ed.* **2021**, *60*, 5811–5815. [CrossRef]
19. Yu, T.; Li, Z.; Jones, W.; Liu, Y.; He, Q.; Song, W.; Du, P.; Yang, B.; An, H.; Farmer, D.M.; et al. Identifying key mononuclear Fe species for low−temperature methane oxidation. *Chem. Sci.* **2021**, *12*, 3152–3160. [CrossRef]
20. Fang, Z.; Murayama, H.; Zhao, Q.; Liu, B.; Jiang, F.; Xu, Y.; Tokunaga, M.; Liu, X. Selective mild oxidation of methane to methanol or formic acid on Fe–MOR catalysts. *Catal. Sci. Technol.* **2019**, *9*, 6946–6956. [CrossRef]
21. Qi, G.S.; Gatt, J.E.; Yang, R.T. Selective catalytic oxidation (SCO) of ammonia to nitrogen over Fe−exchanged zeolites prepared by sublimation of $FeCl_3$. *J. Catal.* **2004**, *226*, 120–128. [CrossRef]
22. Hammond, C.; Dimitratos, N.; Jenkins, R.L.; Lopez−Sanchez, J.A.; Kondrat, S.A.; ab Rahim, M.H.; Forde, M.M.; Thetford, A.; Taylor, S.H.; Hagen, H.; et al. Elucidation and Evolution of the Active Component within Cu/Fe/ZSM−5 for Catalytic Methane Oxidation: From Synthesis to Catalysis. *ACS Catal.* **2013**, *3*, 689–699. [CrossRef]
23. Zuo, H.; Klemm, E. Selective oxidation of methane with H2O2 over Fe−silicalite−1: An investigation of the influence of crystal sizes, calcination temperatures and acidities. *Appl. Catal. A Gen.* **2019**, *583*, 117121. [CrossRef]
24. Zheng, L.; Zhao, Y.; Tang, K.; Ma, C.; Hong, C.; Han, Y.; Cui, M.; Guo, Z. A new experiment station on beamline 4B7A at Beijing Synchrotron Radiation Facility. *Spectrochim. Acta Part B At. Spectrosc.* **2014**, *101*, 1–5. [CrossRef]
25. Rehr, J.J.; Albers, R.C. Theoretical approaches to X-ray absorption fine structure. *Rev. Mod. Phys.* **2000**, *72*, 621–654. [CrossRef]
26. Ravel, B.; Newville, M. Athena, Artemis, Hephaestus: Data analysis for X-ray absorption spectroscopy using IFEFFIT. *J. Synchrotron Rad.* **2005**, *12*, 537–541. [CrossRef] [PubMed]
27. Xie, P.; Luo, Y.; Ma, Z.; Huang, C.; Miao, C.; Yue, Y.; Hua, W.; Gao, Z. Catalytic decomposition of N2O over Fe−ZSM−11 catalysts prepared by different methods: Nature of active Fe species. *J. Catal.* **2015**, *330*, 311–322. [CrossRef]
28. Marturano, P.; Drozdová, L.; Kogelbauer, A.; Prins, R. Fe/ZSM−5 Prepared by Sublimation of FeCl3: The Structure of the Fe Species as Determined by IR, 27Al MAS NMR, and EXAFS Spectroscopy. *J. Catal.* **2000**, *192*, 236–247. [CrossRef]

29. Oda, A.; Aono, K.; Murata, N.; Murata, K.; Yasumoto, M.; Tsunoji, N.; Sawabe, K.; Satsuma, A. Rational design of ZSM−5 zeolite containing a high concentration of single Fe sites capable of catalyzing the partial oxidation of methane with high turnover frequency. *Catal. Sci. Technol.* **2021**, *12*, 542–550. [CrossRef]
30. Zhu, K.; Liang, S.; Cui, X.; Huang, R.; Wan, N.; Hua, L.; Li, H.; Chen, H.; Zhao, Z.; Hou, G.; et al. Highly efficient conversion of methane to formic acid under mild conditions at ZSM−5−confined Fe−sites. *Nano Energy* **2021**, *82*, 105718. [CrossRef]
31. Yu, T.; Su, Y.; Wang, A.; Weckhuysen, B.M.; Luo, W. Efficient Synthesis of Monomeric Fe Species in Zeolite ZSM-5 for the Low-Temperature Oxidation of Methane. *ChemCatChem* **2021**, *13*, 2766–2770. [CrossRef]
32. Kim, M.S.; Park, E.D. Aqueous−phase partial oxidation of methane with H2O2 over Fe−ZSM−5 catalysts prepared from different iron precursors. *Microporous Mesoporous Mater.* **2021**, *324*, 111278. [CrossRef]
33. Hammond, C.; Dimitratos, N.; Lopez−Sanchez, J.A.; Jenkins, R.L.; Whiting, G.; Kondrat, S.A.; ab Rahim, M.H.; Forde, M.M.; Thetford, A.; Hagen, H.; et al. Aqueous−Phase Methane Oxidation over Fe−MFI Zeolites; Promotion through Isomorphous Framework Substitution. *ACS Catal.* **2013**, *3*, 1835–1844. [CrossRef]
34. Schwidder, M.; Kumar, M.S.; Klementiev, K.; Pohl, M.M.; Brückner, A.; Grünert, W. Selective reduction of NO with Fe−ZSM−5 catalysts of low Fe content: I. Relations between active site structure and catalytic performance. *J. Catal.* **2005**, *231*, 314–330. [CrossRef]
35. Santhosh Kumar, M.; Schwidder, M.; Grunert, W.; Bentrup, U.; Brückner, A. Selective reduction of NO with Fe−ZSM−5 catalysts of low Fe content: Part II. Assessing the function of different Fe sites by spectroscopic in situ studies. *J. Catal.* **2006**, *239*, 173–186. [CrossRef]
36. Perez−Ramirez, J.; Kumar, M.S.; Bruckner, A. Reduction of N_2O with CO over Fe−MFI zeolites: Influence of the preparation method on the iron species and catalytic behavior. *J. Catal.* **2004**, *223*, 13–27. [CrossRef]
37. Snyder, B.E.R.; Vanelderen, P.; Bols, M.; Hallaert, S.D.; Böttger, L.H.; Ungur, L.; Pierloot, K.; Schoonheydt, R.A.; Sels, B.F.; Solomon, E.I. The active site of low−temperature methane hydroxylation in iron−containing zeolites. *Nature* **2016**, *536*, 317–321. [CrossRef]
38. Shahami, M.; Shantz, D.F. Zeolite acidity strongly influences hydrogen peroxide activation and oxygenate selectivity in the partial oxidation of methane over M,Fe−MFI (M: Ga, Al, B) zeolites. *Catal. Sci. Technol.* **2019**, *9*, 2945–2951. [CrossRef]
39. Hammond, C.; Jenkins, R.L.; Dimitratos, N.; Lopez−Sanchez, J.A.; Rahim, M.H.A.; Forde, M.M.; Thetford, A.; Murphy, D.M.; Hagen, H.; Stangland, E.E.; et al. Catalytic and Mechanistic Insights of the Low−Temperature Selective Oxidation of Methane over Cu−Promoted Fe−ZSM−5. *Chem. A Eur. J.* **2012**, *18*, 15735–15745. [CrossRef]
40. Choi, S.H.; Wood, B.R.; Ryder, A.J.A.; Bell, A. X-ray Absorption Fine Structure Characterization of the Local Structure of Fe in Fe−ZSM−5. *J. Phys. Chem. B* **2003**, *107*, 11843–11851. [CrossRef]
41. Yu, T.; Li, Z.; Lin, L.; Chu, S.; Su, Y.; Song, W.; Wang, A.; Weckhuysen, B.M.; Luo, W. Highly Selective Oxidation of Methane into Methanol over Cu−Promoted Monomeric Fe/ZSM−5. *ACS Catal.* **2021**, *11*, 6684–6691. [CrossRef]